Design and Analysis of Surface Plasmon Resonance Sensor Based on High-Birefringent Microstructured Optical Fiber

Nancy Meng Ying Zhang[1,2], Dora Juan Juan Hu[3], Perry Ping Shum[1,2], Zhifang Wu[1,2], Kaiwei Li[1], Tianye Huang[1,2] and Lei Wei[1,2,*]

[1]School of Electrical and Electronics Engineering, Nanyang Technological University, Singapore 639798
[2]CINTRA CNRS/NTU/Thales, UMI 3288, 50 Nanyang Drive, Singapore 637553
[3]Institute for Infocomm Research, Agency for Science, Technology and Research, 1 Fusionopolis Way, Singapore 138632

E-mail: WEI.LEI@ntu.edu.sg

Received Month X, XXXX; revised Month X, XXXX; accepted Month X, XXXX; posted Month X, XXXX (Doc. ID XXXXX); published Month X, XXXX

Abstract
Optical fiber based surface plasmon resonance (SPR) sensors are favored by their high sensitivity, compactness, remote and in-situ sensing capabilities. Microstructured optical fibers (MOFs) possess microfluidic channels extended along the entire length right next to the fiber core, thereby enable the infiltrated biochemical analyte to access to the evanescent field of guided light. Since SPR can only be excited by the polarization vertical to metal surface, external perturbation could induce the polarization crosstalk in fiber core, thus leads to the instability of sensor output. Therefore for the first time we analyze how the large birefringence suppresses the impact of polarization crosstalk. We propose a high-birefringent MOF based SPR sensors with birefringence larger than 4×10^{-4} as well as easy infiltration of microfluidic analyte, while maintaining sensitivity as high as 3100 nm/RIU.

Keywords: Surface plasmon resonance, Microstructured optical fiber, Optical fiber sensor

1. Introduction

Surface plasmon resonance (SPR) is considered as one of the most promising techniques in chemical and biochemical sensing due to its excellent sensitivity to the optical properties of ambient dielectric medium. A conventional SPR sensor is implemented on a Kretschmann-Raether glass prism to couple the incident TM-polarized light to surface plasmon polariton (SPP) that propagates parallel to the interface of thin metal layer that deposited on prism base and semi-infinite dielectric medium when the phase matching condition is satisfied [1]. Due to the limitations of bulky and non-flexible geometry of prism based SPR sensors, researchers have been seeking approaches using optical fibers [2]. Optical fiber based SPR sensors possess advantages of miniaturization, remote sensing and in-situ monitoring [3]. Many optical fiber structures have been proposed for SPR sensing such as tapered fiber [4], D-shaped fiber [5], U-shaped fiber [6] and fiber gratings [7, 8]. In recent years, SPR sensors that are based on microstructured optical fiber (MOF) has drawn growing interests [9]. MOFs are recognized by their fine arrangement of air holes in cladding region extended along the entire fiber length. Solid core MOFs can achieve small core dimensions with much better robustness and flexibility than tapered fibers and striped fibers. Gas or liquid analyte can be infiltrated into the cladding air holes around fiber core and approaches to the strong evanescent field of guided mode due to the small core dimension. This unique feature realizes effective excitation of SPP when coating thin metal layers on the inner walls of cladding air holes. Several structures of MOFs have been proposed for SPR sensor, such as hexagonal solid core MOF [10], semicircular channel MOF [11], birefringent photonic crystal fiber (PCF) [12], multi-channel PCF [13] and suspended core MOF [14]. However, two orthogonal polarizations of

guided mode can be coupled to each other when external perturbation such as bending, twisting or pressure is applied to fiber. Birefringence exists in most designs of MOF based SPR sensors [11-14] due to the structural asymmetry in two orthogonal polarization directions. Hence the resonant wavelengths corresponding to two orthogonal polarizations separate yet their transmission dips overlap partially. Since SPP can only be excited by TM-polarized light, most SPR sensors monitor the transmission spectrum of the polarization that excites strongest surface plasmon wave. External perturbations or inaccurate input polarization would lead to the existence of undesired polarization thereby a shifted resonant wavelength. To address the wavelength offset, we propose a SPR sensor that based on a so-called polarization-maintaining MOF (PM-MOF) which is intentionally introduced with high birefringence in fiber structure, so that the SPR behaviors of two orthogonal polarization modes are well distinct. For the first time, we analyze the relation between birefringence and wavelength offset and present the requisite birefringence to suppress the impact of polarization crosstalk. The proposed PM-MOF has a near-panda structure that provides desirable birefringent properties while maintaining feasibility in fabrication. It can be fabricated by the stack-and-draw method which is used in MOF manufacturing. The high-birefringent structure can provide comparable sensitivity of previously reported MOF based SPR sensors. More importantly, the high-birefringent MOF can minimize the polarization crosstalk therefore improve the stability of SPR sensor.

2. Theory

In the configuration of Kretschmann-Raether prism, SPR is generated when the propagation constant of evanescent wave that parallel to metal-dielectric interface equals to the propagation constant of SPP, which is known as the phase matching condition [15]:

$$\frac{\omega}{c}\sqrt{\varepsilon_{prism}}\sin(\theta_{res}) = \frac{\omega}{c}\sqrt{\frac{\varepsilon_{metal}\varepsilon_{dielectric}}{\varepsilon_{metal}+\varepsilon_{dielectric}}} + \Delta\beta \quad (1)$$

where θ_{res} is the angle of incidence at which the SPR occurs. ε_{prism}, ε_{metal} and $\varepsilon_{dielectric}$ are the dielectric constants of prism material, metal layer and dielectric medium, respectively. The left expression of equation (1) defines the propagation constant of evanescent wave of TM-polarized light with incidence angle θ_{res} at the prism-air interface. The first term of right expression of equation (1) defines the propagation constant of SPP obtained by solving Maxwell's equations for the interface of semi-infinite metal and dielectic media. The second term $\Delta\beta$ denotes the effects of finite thickness of metal layer and the high refractive index of prism. $\Delta\beta$ is much smaller compared with the first term thus it is often neglected [16]. It decreases when the metal film thickness increases [15]. This principle can also be applied to optical fiber based SPR sensor, except that the angle of incidence in optical fiber shall vary from the critical angle to 90° [9]. It can be concluded from equation (1) that when the phase matching condition is satisfied, the effective refractive index of the guided mode in optical fiber equals to that of the surface plasmon mode [17].

The resonant dip of SPR sensor corresponds to the largest transmission loss of the guided mode. The attenuation of core mode L_c (dB/m) in optical fiber is given by [18]:

$$L_c = 8.686 \times k_0 Im(n_{eff}) \quad (2)$$

where k_0 is the free space wave vector and Im(n_{eff}) is the imaginary part of effective refractive index of core mode. Therefore, the sensor measurement can be realized by monitoring the variation of L_c, which is a function of Im(n_{eff}).

In this work we adopt the wavelength interrogation method, in which the shift of resonant wavelength corresponding to the peak transmission loss induced by the change of refractive index of analyte is followed to evaluate the SPR sensor performance. The sensitivity of SPR sensor S_λ (nm/RIU) can be approximated by the following expression [15]:

$$S_\lambda = \frac{\delta\lambda}{\delta n_a} = \frac{n_p\varepsilon_{mr}}{\frac{n_p}{\lambda}n_a^3\left(\frac{1}{\varepsilon_{mr}}-1\right)+\frac{dn_p}{d\lambda}n_a\left(n_a^2+\varepsilon_{mr}\right)} \quad (3)$$

where n_a and n_p are the refractive indices of analyte and prism respectively. ε_{mr} is the real part of dielectric constant of thin metal layer in the SPR configuration.

3. Configuration and Principles

We propose a SPR sensor based on a near-panda MOF with three rings of photonic crystal air holes (figure 1 (a)). The pitch of MOF is 3.94 μm. The diameters of two central air holes in lateral direction are enlarged to be 2.5 times of those of the others. The diameters of small holes and large holes are d_1 = 1.75 μm and d_2 = 4.38 μm, respectively. We coat gold layers on the inner walls of two large central holes and fill these two holes with analyte. We numerically analyze the behaviors of proposed SPR sensor using COMSOL which conducts modeling with finite element method (FEM). FEM meshes the constructed geometry into triangular elements with different sizes and refractive indices [19]. The maximum and minimum element sizes at the boundaries of gold layers are

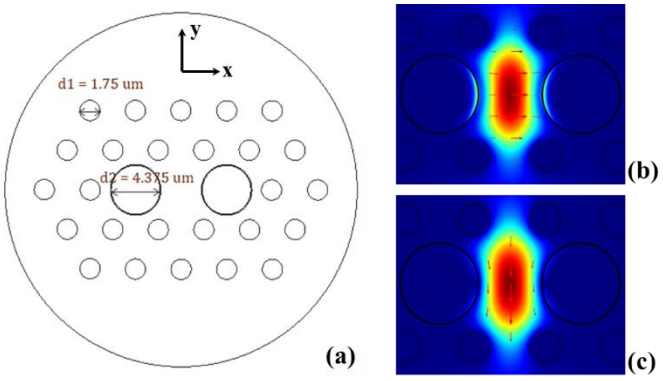

Figure 1. (a) Schematic structure of near-panda MOF based SPR sensor; (b) x-polarized and (c) y-polarized core mode pattern of proposed SPR sensor.

0.05 μm and 0.45 nm, respectively. The remaining parts of geometry use the fine mesh that is predefined by COMSOL. A peripheral layer of 3 μm thick is added as the perfectly matched layer (PML) to avoid interference by the reflection at geometry boundary. The material of MOF is fused silica, of which the refractive index can be determined by the Sellmeier equation. The dielectric constant of gold is characterized by the Drude-Lorentz model [20]. The core mode pattern with polarization in lateral direction that primarily excites the surface plasmon on the surface of gold layer is shown in figure 1 (b).

Figure 2 shows the variations of the effective indices of x-polarized core mode and surface plasmon (SP) mode of the MOF. According to equation (1), the intersection of the real part of core mode index and real part of SP mode index indicates the equating of the propagation constants, at which phase matching condition is satisfied. However at near infrared (IR) wavelengths, the effective refractive index of surface plasmon mode would be closed to the bordering analyte, e.g. ~1.33, which is much lower than that of a

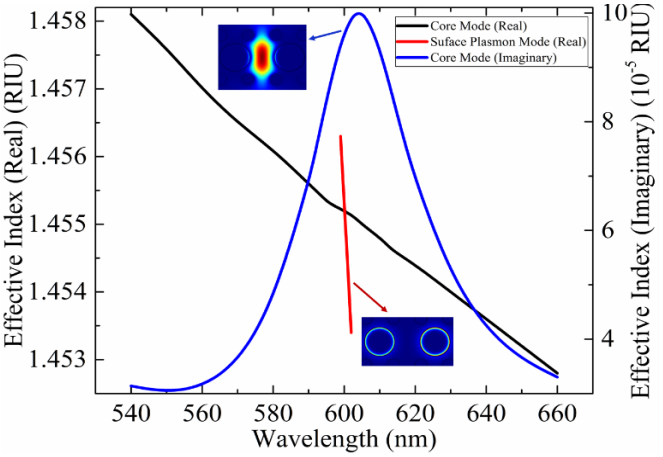

Figure 2. Effective indices of core mode and surface plasmon mode with refractive index of analyte of 1.33 and gold layer thickness of 70 nm.

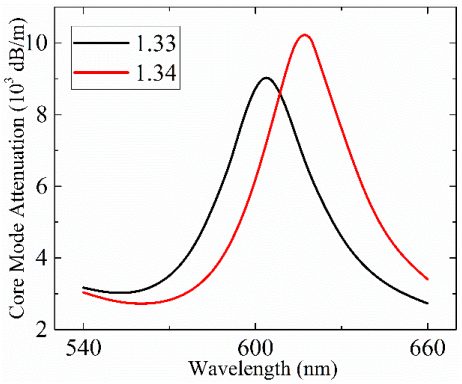

Figure 3. Changes of core mode transmission loss when refractive index of analyte increases from 1.33 to 1.34.

silica fiber [1]. Hence the operating wavelengths of SPR sensor is ~600 nm where the indices of core mode and surface plasmon mode equate at ~1.45. Based on equation (2), core mode attenuation L_c is a function of Im(n_{eff}). We follow the shift of resonant wavelength at which L_c is largest to evaluate the sensitivity of proposed sensor.

Figure 3 presents the obvious redshift and the enhancement of peak transmission loss when the refractive index of infiltrated analyte increases from 1.33 to 1.34. The resonant wavelength shifts from 604 nm to 617 nm.

4. Discussion

The proposed fiber structure with two enlarged central holes introduces large birefringence that improves the immunity of sensor output to polarization crosstalk. Considering a conventional hexagonal lattice solid core PCF with cladding air hole diameter of 1.75 μm and pitch of 3.94 μm, SPP can be excited by both x- and y-polarized guide modes due to the cylindrical geometry of thin metal layers coated on the inner walls of first ring air holes. As shown in figure 4, SPP is mainly excited on the metal layer surfaces that normal to the polarization direction. Birefringence commonly exists in structures of MOF based SPR sensors. Hence SPR corresponding to x- and y-polarized modes show divergent wavelengths and intensities. As a result, when

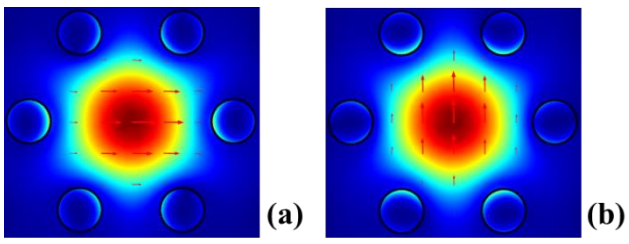

Figure 4. Mode patterns of (a) x- and (b) y-polarized core mode in conventional PCF with 50 nm gold layers and analyte refractive index of 1.38.

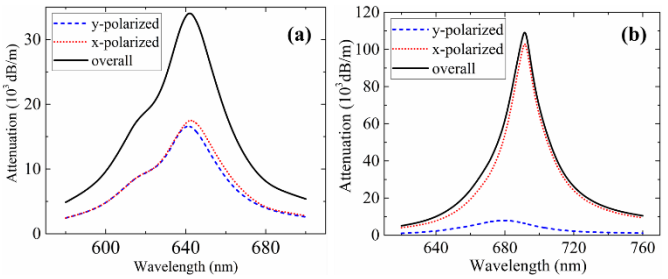

Figure 5. Loss spectra of MOF based SPR sensors when (a) d_1/d_2=0.95 (b) d_1/d_2=0.4 with analyte refractive index of 1.38.

input polarization is not at the exact wanted direction or external perturbation leads to polarization crosstalk so that two orthogonal polarizations coexist, the overall detected SPR signal would be offset. To analyze how the birefringence influences resonant wavelength offset, we gradually enlarge the two central holes in lateral direction of the structure shown in figure 1 to introduce birefringence intentionally.

Figure 5 (a) shows the loss spectra of MOF based SPR sensor when the ratio of common air hole diameter d_1 and two enlarged central holes diameter d_2 is 0.95. The inner walls of first ring air holes are coated with 50 nm gold films. The refractive index of infiltrated analyte is 1.38, which is the typical effective refractive index of cytoplasm [21-23] and some types of protein layers [24, 25]. When d_1/d_2 = 0.95, the modal birefringence at resonant wavelength is ~2×10^{-5}. As shown in Figure 5 (a), the resonant wavelengths of x- and y-polarized core modes are 642.66 nm and 641.19 nm respectively and the attenuation corresponding to two polarizations are similar. The resonance of total loss spectrum is at 641.99 nm, which shifts 0.67 nm from that of x-polarized mode. Hence when the unwanted y-polarization is induced by external

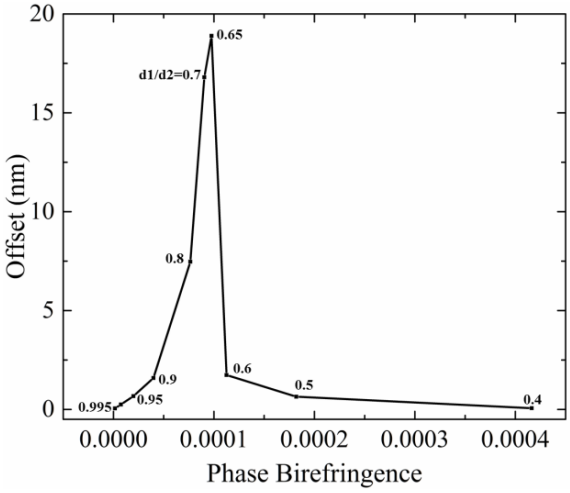

Figure 6. Resonant wavelength offset against phase birefringence.

perturbation, the 0.67 nm resonant wavelength offset compromises the accuracy of SPR sensor output. Figure 5 (b) shows the loss spectra of our proposed PM-MOF. The high-birefringent structure enlarges SPP of x-polarized core mode while significantly suppresses SPP of y-polarized mode. Although the resonant wavelengths of two polarizations are more drifted apart, the overall loss spectrum is predominated by that of x-polarized mode. The resonant wavelength offset is improved to be as small as 0.06 nm. The phase birefringence at resonant wavelength is ~4.2×10^{-4}.

The resonant wavelength offset undergoes a rise and fall along with the increasing birefringence as the two central holes expanding (figure 6). When d_1/d_2 varies from 0.9 to 0.65 meanwhile birefringence increases from ~4×10^{-5} to ~1×10^{-4}, the wavelength offset increases to be as high as 18.89 nm. After birefringence exceeds ~1×10^{-4}, the offset sharply drops and tends towards 0 beyond birefringence of ~4×10^{-4}. The resonant wavelength of overall loss spectrum is determined by the phase birefringence and the relative magnitude of the attenuation of x- and y-polarized modes. When birefringence is relatively small, i.e. d_1/d_2 > 0.65, the overall resonant wavelength is drifted away from that of x-polarized mode due to the considerably large influence of y-polarized mode as the relative magnitude is not significant. After a threshold, i.e. d_1/d_2 = 0.65, the overall resonant wavelength shifts towards that of x-polarized mode. Since the loss spectrum of y-polarized mode is much smaller than that of x-polarized mode at large birefringence, the overall loss spectrum is predominated by x-polarized mode. Therefore even if the resonant wavelengths of two orthogonal modes continue drifting apart, the influence of y-polarized mode becomes too small that the overall resonant wavelength quickly shifts towards that of x-polarized mode. This is why the offset suddenly drops after the

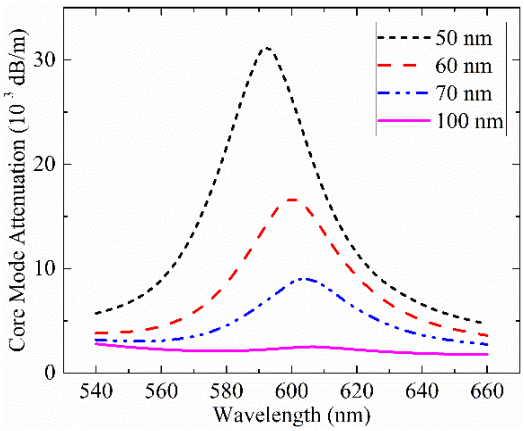

Figure 7. Variations of core mode attenuation with filled analyte refractive index of 1.33 when the thickness of gold layers is 50 nm, 60 nm, 70 nm and 100 nm respectively.

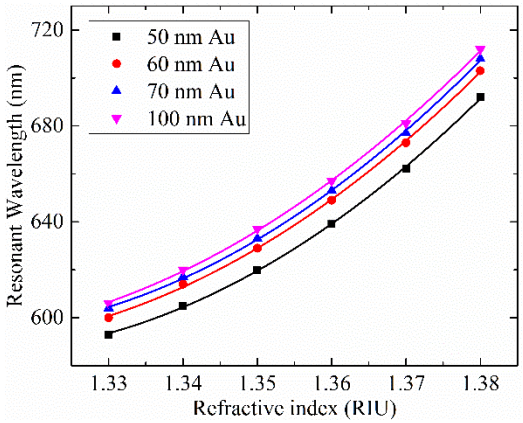

Figure 8. Sensitivities as a function of resonant wavelength shift when thickness of gold layers is 50 nm, 60 nm, 70 nm and 100 nm respectively.

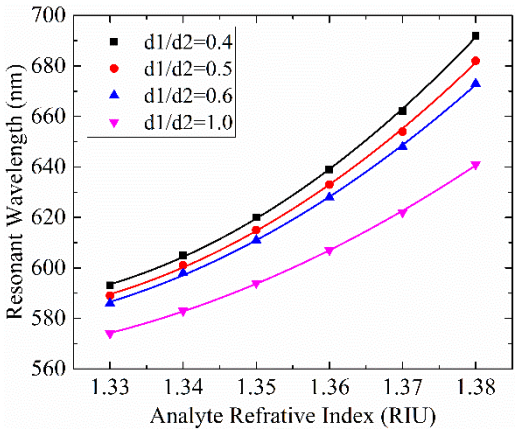

Figure 9. Effects of the dimension of central enlarged holes on sensitivity.

ratio exceeds 0.65.

Figure 6 indicates that a birefringence larger than 2×10^{-4} can effectively reduce the resonant wavelength offset thereby enhance the resistance of wavelength interrogation to polarization crosstalk. Our proposed MOF provides modal birefringence as high as $\sim4.2\times10^{-4}$ that suppresses the offset to be extremely small.

The thickness of metal layer is very crucial to surface plasmon excitation. Both the peak transmission loss and the resonant wavelength can be affected by the change of gold layer thickness. We investigate the impact of gold layer thickness on the attenuation spectrum and the sensitivity of proposed SPR sensor. Figure 7 shows the attenuation spectra of proposed sensor with analyte refractive index of 1.33 when the gold layer thickness is 50 nm, 60 nm, 70 nm and 100 nm respectively. As the gold layer thickens, the resonance shifts to longer wavelengths and the transmission loss significantly reduces especially when the gold thickness increases from 50 nm to 60 nm. The phenomenon agrees well with previous studies [26, 27]. It has been proven that when the gold layer thickness increases from 0 to 60 nm, the SPR loss first rises and then declines. The highest loss of SPR appears at thickness of ~22 nm, beyond which the electric field has difficulty to penetrate through the gold layer. The decline rate of resonance loss due to the gold layer thickening slows down as the gold thickness exceeds ~40 nm [17]. Since the term $\Delta\beta$ in equation (1) decreases with the metal layer thickening [15], the thickening of gold layer leads to the decrease of real part of effective index of surface plasmon mode. As a result, the phase matching between the fiber core mode and surface plasmon mode is satisfied at a smaller effective refractive index thereby a longer resonant wavelength. That is the reason why we observe a redshift of resonant wavelength as gold thickness increases.

Although the intensity of surface plasmon wave is highly impacted by the thickness of gold layer, the sensitivities of proposed SPR sensors are weakly affected as the gold thickness changes (figure 8). Within a relatively wide refractive index range from 1.33 to 1.38, the resonant wavelength exhibits polynomial increase. The larger the refractive index of analyte, the higher the sensitivity is. This property of SPR sensor can be explained by equation (3). The denominator of equation (3) consists of two terms with opposite signs since the material dispersion of optical fiber in the second term, $dn_p/d\lambda$, is negative. Although the second term slightly increases as the wavelength increases, the overall effect is dominated by the first term so that the sensitivity is higher at longer wavelength, which corresponds to larger refractive index of analyte. As shown in figure 8, the sensitivities curves of 50 nm, 60 nm, 70 nm and 100 nm gold thickness are nearly in parallel. Hence the sensitivity is weakly affected by the gold layer thickness. This is reasonable since the variables in equation (3) are weakly impacted by the change of metal layer thickness. Similar phenomenon is also observed in [28]. The sensitivity of SPR sensor can be viewed as linear within small refractive index range (e.g. 1.37 - 1.38). The larger the refractive index, the higher the sensitivities are. Within the refractive index of 1.37 - 1.38, the sensitivities corresponding to 50 nm, 60 nm, 70 nm and 100 nm gold thickness are 3000 nm/RIU, 3000 nm/RIU, 3100 nm/ RIU and 3100 nm/RIU respectively.

Besides birefringence, the large two central holes dimension also improves the sensor sensitivity. We compare the sensitivities of dimensions that $d_1/d_2 = 0.4$, $d_1/d_2 = 0.5$, $d_1/d_2 = 0.6$ with only two enlarged holes coated with 50 nm gold layers and infiltrated with

analyte and the sensitivity of conventional PCF shown in figure 4. It can be seen from figure 9 that larger two central holes provide higher sensitivity especially at high refractive index range. The sensitivities are 1900 nm/RIU, 2500 nm/RIU, 2800 nm/RIU and 3000 nm/RIU within refractive index of 1.37 - 1.38, corresponding to d_1/d_2 = 1.0, 0.6, 0.5 and 0.4, respectively. The improvement of sensitivity along with holes expanding is mainly due to the increased interaction area between the core mode and the infiltrated analyte as well as the enhanced evanescent field owing to smaller core dimension in lateral direction. Hence our birefringent structure provides a higher SPR sensitivity compared with other hexagonal latticed non-birefringent MOFs [29-31].

5. Conclusions

In conclusion, we demonstrate the capability of using easily fabricated high-birefringent MOF to construct reliable and sensitive SPR sensors. Our simulation results show the enhancement of birefringence and the optimization of the detection sensitivity can be made by tuning the structural parameters. The large area of air holes around the fiber core leads to high birefringence that effectively suppresses polarization crosstalk, and also enables easy microfluidic infiltration as well as enhances the interaction between SPP and analyte. The proposed sensor offers advantage in stabilizing SPR sensing performance under polarization crosstalk, while providing sensitivity as high as 3100 nm/RIU.

6. Acknowledgement

This work is supported in part by the Singapore Ministry of Education Academic Research Fund Tier 2 (MOE2015-T2-1-066), and Nanyang Technological University (Startup grant: Lei Wei).

References

[1] Gauvreau B, Hassani A, Fassi Fehri M, Kabashin A and Skorobogatiy M A 2007 Photonic bandgap fiber-based surface plasmon resonance sensors *Opt. Exp.* **15** 11413-11426.

[2] Sharma A K and Gupta B D 2006 Theoretical model of a fiber optic remote sensor based on surface plasmon resonance for temperature detection *Opt. Fiber Technol.* **12** 87-100.

[3] Guo X 2012 Surface plasmon resonance based biosensor technique: a review *J. Biophotonics* **5** 483-501.

[4] Verma R K, Sharma A K and Gupta B D 2008 Surface plasmon resonance based tapered fiber optic sensor with different taper profiles *Opt. Commun.* **281** 1486-1491.

[5] Chiu M H, Wang S F and Chang R S 2005 D-type fiber biosensor based on surface-plasmon resonance technology and heterodyne interferometry *Opt. Lett.* **30** 233-235.

[6] Verma R K and Gupta B D. 2008 Theoretical modelling of a bi-dimensional U-shaped surface plasmon resonance based fibre optic sensor for sensitivity enhancement *J. Phys. D Appl. Phys.*, **41** 095106.

[7] Schuster T, Herschel R, Neumann N and Schäffer C G 2012 Miniaturized long-period fiber grating assisted surface plasmon resonance sensor *J. Lightw. Technol.* **30** 1003-1008.

[8] Shevchenko Y Y and Albert J 2007 Plasmon resonances in gold-coated tilted fiber Bragg gratings *Opt. Lett.* **32** 211-213.

[9] Zhao Y, Deng Z Q and Li J 2014 Photonic crystal fiber based surface plasmon resonance chemical sensors *Sensor. Actuat. B-Chem.* **202** 557-567.

[10] Zheng L, Zhang X, Ren X, Wang Y, Liu X and Huang Y 2009 A comparison of Au and Ag metalized layer in microstructured optical fibers for surface plasmon resonance excitation *Asia Communications and Photonics* 763419-763419.

[11] Hassani A and Skorobogatiy M 2006 Design of the microstructured optical fiber-based surface plasmon resonance sensors with enhanced microfluidics *Opt. Exp.* **14** 11616-11621.

[12] Otupiri R, Akowuah E K, Haxha S, Ademgil H, AbdelMalek F and Aggoun A 2014 A novel birefrigent photonic crystal fiber surface plasmon resonance biosensor *IEEE Photon. J.* **6** 1-11.

[13] Akowuah E K, Gorman T, Ademgil H, Haxha S, Robinson G K and Oliver J V 2012 Numerical analysis of a photonic crystal fiber for biosensing applications *IEEE J. Quantum Electron.* **48** 1403-1410.

[14] Hautakorpi M, Mattinen M and Ludvigsen H 2008 Surface-plasmon-resonance sensor based on three-hole microstructured optical fiber *Opt. Exp.* **16** 8427-8432.

[15] Homola J 1997 On the sensitivity of surface plasmon resonance sensors with spectral interrogation *Sensor. Actuat. B-Chem.* **41** 207-211.

[16] Gupta B D and Verma R K 2009 Surface plasmon resonance-based fiber optic sensors: principle, probe designs, and some applications *J. Sensors* **2009** 979761.

[17] Yu X, Zhang Y, Pan S, Shum P, Yan M, Leviatan Y and Li C 2010 A selectively coated photonic crystal fiber based surface plasmon resonance sensor *J. Opt.* **12** 015005.

[18] Tan Z, Li X, Chen Y and Fan P 2014 Improving the sensitivity of fiber surface plasmon resonance sensor by filling liquid in a hollow core photonic crystal fiber *Plasmonics* **9** 167-173.

[19] Cucinotta A, Selleri S, Vincetti L and Zoboli M 2002 Holey fiber analysis through the finite-element method *IEEE Photon. Technol. Lett.* **14** 1530-1532.

[20] Vial A, Grimault A S, Macías D, Barchiesi D and de La Chapelle M L 2005 Improved analytical fit of gold dispersion: Application to the modeling of extinction spectra with a finite-difference time-domain method," *Phys. Rev. B.* **71**.

[21] Meglinski I and Doronin A 2013 Monte Carlo modeling of photon migration for the needs of biomedical optics and biophotonics *Series in Optics and Optoelectronics* **19** 1-58.

[22] Liang X J, Liu A Q, Lim C S, Ayi T C and Yap P H 2007 Determining refractive index of single living cell using an integrated microchip *Sensor. Actuat. A-Phys.* **133** 349-354.

[23] Khan S, Pierce D and Vale R D 2000 Interactions of the chemotaxis signal protein CheY with bacterial flagellar motors visualized by evanescent wave microscopy *Curr. Biol.* **10** 927-930.

[24] Psarouli A, Salapatas A, Botsialas A, Petrou P S, Raptis I, Makarona E, Jobst G, Tukkiniemi K, Sopanen M, Stoffer R and Kakabakos S E 2015 Monolithically integrated broad-band Mach-Zehnder interferometers for highly sensitive label-free detection of biomolecules through dual polarization optics *Sci. Rep.* **5** 17600.

[25] Nguyen T T, Bea S O, Kim D M, Yoon W J, Park J W, An S S A and Ju H 2015 A regenerative label-free fiber optic sensor using surface plasmon resonance for clinical diagnosis of fibrinogen *Int. J. Nanomedicine* **10** 155.

[26] Suzuki H, Sugimoto M, Matsui Y and Kondoh J 2008 Effects of gold film thickness on spectrum profile and sensitivity of a multimode-optical-fiber SPR sensor *Sensor. Actuat. B-Chem.* **132** 26-33.

[27] Hassani A and Skorobogatiy M 2007 Design criteria for microstructured-optical-fiber-based surface-plasmon-resonance sensors *J. Opt. Soc. Amer. B.* **24** 1423-1429.

[28] Zheng L, Zhang X, Ren X, Wang Y, Liu X and Huang Y 2009 A comparison of Au and Ag metalized layer in microstructured optical fibers for surface plasmon resonance excitation *Asia Communications and Photonics* 763419-763419.

[29] Wei W, Zhang X, Guo X, Zheng L, Gao J, Shi W, Wang Q, Huang Y and Ren X 2012. Refractive index sensors based on Ag-metalized nanolayer in microstructured optical fibers *Optik* **123** 1167-1170.

[30] Bing P, Yao J, Lu Y and Li Z 2012 A surface-plasmon-resonance sensor based on photonic-crystal-fiber with large size microfluidic channels *Opt. Appl.* **42** 493-501.

[31] Zheng L, Zhang X, Ren X, Gao J, Shi L, Liu X, Wang Q and Huang Y 2011 Surface plasmon resonance sensors based on Ag-metalized nanolayer in microstructured optical fibers *Opt. Laser Technol.* **43** 960-964.